Lozano-Torres, B.; Blandez, JF.; Galiana, I.; García-Fernández, A.; Alfonso-Navarro, M.; Marcos Martínez, MD.; Orzáez, M.... (2020). Real-Time In Vivo Detection of Cellular Senescence through the Controlled Release of the NIR Fluorescent Dye Nile Blue. Angewandte Chemie International Edition. 59(35):15152-15156. https://doi.org/10.1002/anie.202004142

Real time *in vivo* detection of cellular senescence through the controlled release of the NIR fluorescent dye Nile Blue

Beatriz Lozano-Torres,[a],[b],[c],[d],† Juan F. Blandez,[a],[b],[d],† Irene Galiana,[a],[b] Alba García-Fernández,[c] María Alfonso,[a] María D. Marcos,[a],[b],[c],[d] Mar Orzáez,[b],[e] Félix Sancenón,[a],[b],[c],[d]* and Ramón Martínez-Máñez[a],[b],[c],[d]*

Abstract: *In vivo* optical detection of cellular senescence is accomplished by using mesoporous silica nanoparticles loaded with the NIR-FDA approved Nile Blue (**NB**) dye and capped with a galactohexasaccharide (**S3**). Emission at 672 nm of **NB** is highly quenched inside **S3**, yet a remarkable emission enhancement is observed upon cap hydrolysis in the presence of β-galactosidase and dye release. The efficacy of the probe to optically detect cellular senescence is tested *in vitro* in melanoma SK-Mel-103 and breast cancer 4T1 cells and *in vivo* in palbociclib-treated BALB/cByJ mice bearing breast cancer tumor.

Cellular senescence is a stable state of cell cycle arrest necessary for maintaining the organism homeostasis.[1] However, the improper elimination of senescent cells, provokes local inflammation, tissue degeneration and contributes to aging.[2] Today scientific evidence supports that accumulation of senescent cells is involved in the pathophysiology of many age-related diseases[3] and has boosted the concept that senescent cells is an attractive therapeutic target.[4,5] Recent reports, using *in vivo* models, evidence that a wide variety of diseases can be ameliorated by the elimination of senescent cells.[6,7]

Characteristic signs of cellular senescence include changes in cell morphology,[8] the appearance of condensed nuclear chromatin foci, known as senescence-associated heterochromatic foci (SAHF).[9] and the overexpression or activation of tumor supressor proteins such as p53, $p16^{INK4a}$ and p21 that contribute to cell cycle arrest.[10] Moreover, one of the most widely used markers to detect celular senescence is the overexpression of lysosomal β-galactosidase, also referred to as senescence-associated β-galactosidase (SA-β-Gal).[11] Measurement of SA-β-Gal activity using chromo-fluorogenic probes has become popular as an easy and simple procedure to detect senescence.[12,13] The use of molecularly imprinted nanopartilces has also been described recently for senescence detection.[14,15] However, most of the actual probes are suitable for *in vitro* studies, whereas probes to detect cellular senescence *in vivo* in realistic senescence models are scarce. One general drawback of most of these probes is that, even in realistic senescence models, detection is only posible after the animal sacrifice. Consequently, the development of suitable methods for *in vivo* senescence detection remains an unresolved problem.[2]

Based on the above, we report herein the use of nanoparticles[16] for *in vivo* detection of cellular senescence using a NIR fluorophore. The probe consists of galactohexasaccharide-capped mesoporous silica nanoparticles (MSNs) which are able to release their cargo in senescent cells due to the hydrolysis of the capping oligosaccharide by SA-β-Gal.[17] We tested a number of fluorophores as cargo and finally selected Nile Blue (**NB**) due to its remarkable features as *in vivo* imaging agent. **NB** is an organic dye approved by the Food and Drug Administration (FDA) for human use[18] and it exhibits near infrared (NIR) emission at 672 nm.[19,20] Most importantly, **NB** is an aromatic planar fluorophore, which is highly quenched at high concentrations or in confined spaces as it forms non-emissive π-stacked aggregates.[21]

MSNs have been widely used as drug delivery systems due to their properties, such as biocompability and easy functionalization.[22] In addition to MSNs, other carriers for cargo delivery such as liposomes, micelles, polymers, etc have also been used in recent years.[23] In our case, MSNs were chosen as nanocarriers, due to their high loading capacity, allowing the **NB** dye to be entrapped at high concentration resulting in effective dye-dye π-stacking interactions and quenching. This compact packaging together with the gating capability exerted by the capping galactohexasaccharide (*vide infra*) would hardly be obtained using other nanocarriers. In fact, MSNs are well suited for the preparation of on-command delivery carriers by the functionalization of the outer surface with (bio)molecules that prevent payload release unless exposed to specific stimuli.[23] Besides, in MSN the cargo is simply encapsulated, while in some other nanoparticles cargo molecules need to be covalently linked.

The prepared nanoparticles (i.e. **S3** in Figure 1) are therefore poorly emissive, yet SA-β-Gal-induced hydrolysis of the capping hexagalacto-saccharide to give galactose residues, is expected to result in **NB** release, selectively inducing a marked NIR emission enhancement in senescent cells. Targeting of senescent cells *in vitro* with **S3** is validated in SK-Mel-103 (human melanoma) and 4T1 (murine breast cancer) cell lines treated with palbociclib. Moreover, *in vivo* detection of cellular senescence is demonstrated in BALB/cByJ mice bearing

[a] B. Lozano-Torres, Dr. J. F. Blandez, I. Galiana, Dr. M. Alfonso, Prof. M. D. Marcos, Dr. F. Sancenón, Prof. R. Martínez-Máñez
Instituto Interuniversitario de Investigación de Reconocimiento Molecular y Desarrollo Tecnológico (IDM), Universitat Politècnica de València, Universitat de València. Camino de Vera s/n, 46022-Valencia, Spain. E-mail: rmaez@qim.upv.es

[b] B. Lozano-Torres, Dr. J. F. Blandez, I. Galiana, Prof. M. D. Marcos, Dr. M. Orzaez, Dr. F. Sancenón, Prof. R. Martínez-Máñez
Unidad Mixta UPV-CIPF de Investigación en Mecanismos de Enfermedades y Nanomedicina, Universitat Politècnica de València, Centro de Investigación Príncipe Felipe, Valencia, Spain.

[c] B. Lozano-Torres, Alba García-Fernandez, Prof. M. D. Marcos, Dr. F. Sancenón, Prof. R. Martínez-Máñez
CIBER de Bioingeniería, Biomateriales y Nanomedicina (CIBER-BBN).

[d] B. Lozano-Torres, Dr. J. F. Blandez, Prof. M. D. Marcos, Dr. F. Sancenón, Prof. R. Martínez-Máñez
Unidad Mixta de Investigación en Nanomedicina y Sensores. Universitat Politècnica de València, IIS La Fe, Valencia, Spain.

[e] Dr. M. Orzaez
Centro de Investigación Príncipe Felipe. Eduardo Primo Yúfera, 3. Valencia 46012, Spain.

† Both authors contributed equally to this work

breast cancer tumor treated with senescence-inducing chemotherapy.

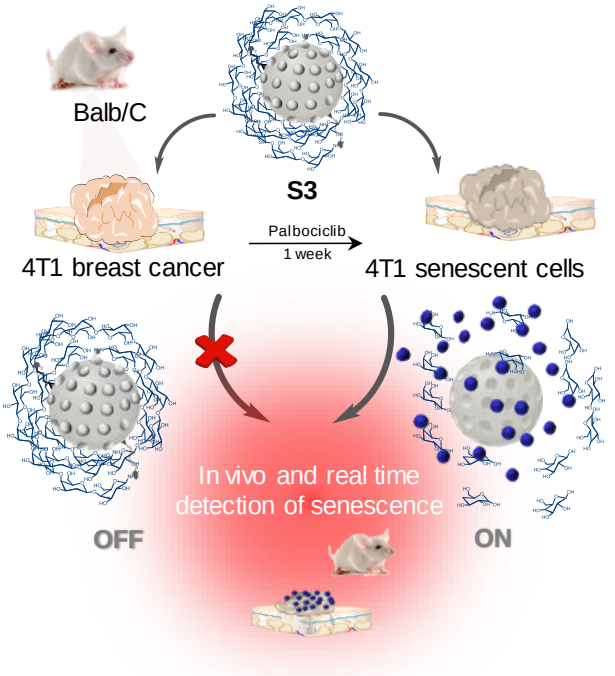

Figure 1. Representation of **S3** activation in BALB/cByJ female mice orthotopically injected with 4T1 cells to generate breast tumors. After tumor formation, mice were administered with palbociclib to generate senescence and treated with **S3** achieving *in vivo* detection of cellular senescence.

S3 is easily prepared from mesoporous silica nanoparticles,[24] which are loaded with **NB**, externally functionalized with APTES and finally capped with β(1,4)-hexagalacto-saccharide (Scheme S1).The mesoporous structure in **S3** and the starting mesoporous silica material (**S0**) was clearly observed by HR-TEM (Figure 2a, b and S1a) and by powder X-ray diffraction (Figure S1b). **S3** was also characterized by porosimetry (Figure S2a, b and Table S1), ATR (Figure S3) and DLS (Figure S4). Moreover, from dye delivery experiments and thermogravimetric studies, the content of **NB** in **S3** was determined to be 0.45 mmol g^{-1} of solid (Figure S5).

Quenching of **NB** inside the pores of **S3**, was assessed. Free **NB** solutions presented much higher fluorescence than suspensions of **S3**, which showed negligible emission at equivalent **NB** concentrations (Figure 2c). Moreover, confocal images of **S3** demonstrated that capped nanoparticles were poorly emissive (Figure S6). Quenching of **NB** at high concentrations was also studied in solution by monitoring the emission of the fluorophore at 666 nm (λ_{exc} = 635 nm) at different **NB** concentrations in water (pH = 4.5)-DMSO 99:1 v/v mixtures. Emission of **NB** solutions increased until a concentration of ca. 1.0 x 10^{-4} M, whereas at higher concentrations the fluorescence decreased. In fact, **NB** concentrations higher than 10^{-3} M are poorly emissive (Figure 2d). From the amount of **NB** loaded and the specific pore volume in **S3** a molar concentration of the dye in the pores of ca. 0.49 M was calculated which is in agreement with the low emission observed for **S3** in Figure 2c.

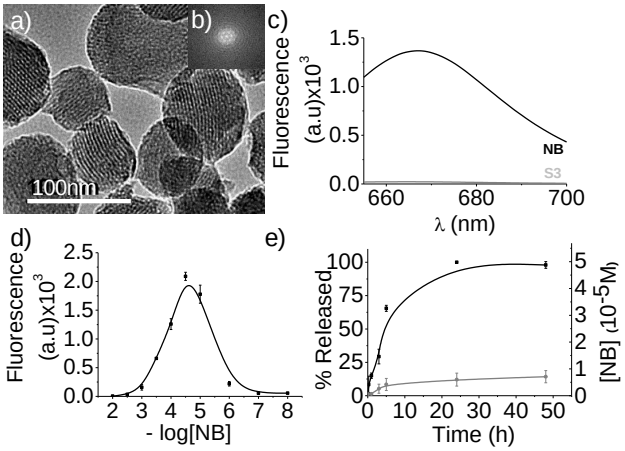

Figure 2. (a) HR-TEM images of **S3**, (b) TEM-EDX of **S3**. (c) Fluorescence of a **NB** solution (1.81 x 10^{-4} M) and of **S3** suspensions at equivalent concentrations of the dye. (d) Emission intensity of **NB** solutions *vs* fluorophore concentration. (e) Release profile of **S3** in the absence (grey line) and in the presence of β-Gal (black line). Experiments were carried out in water-DMSO 99:1 v/v mixtures at pH 4.5. Error bars are expressed as 3σ

Delivery of **NB** from **S3** was studied in the presence and in the absence of β-Gal enzyme (Figure 2e). **S3** show a marked **NB** delivery in the presence of β-Gal of ca. 90% of the maximum dye released after 24 h, which corresponded to 31.4 % (5.69 x 10^{-5} M) of the dye entrapped (Figure S7). In contrast a low **NB** release in the absence of β-Gal was found. Release in the presence of β-Gal is due to the hydrolysis of glycosidic bonds in the capping galacto-saccharide which reduced steric crowding around the pores allowing **NB** delivery.

Specific targeting of senescent cells *in vitro* with **S3** was demonstrated in SK-Mel-103 (human melanoma) and 4T1 (murine breast cancer) cells treated with 5 μM palbociclib (a CDK4/6 inhibitor which suppresses DNA replication inducing cell cycle arrest) for two weeks to induce senescence. Senescence was confirmed by X-Gal staining (Figures 3a,3e, 3i and 3m).

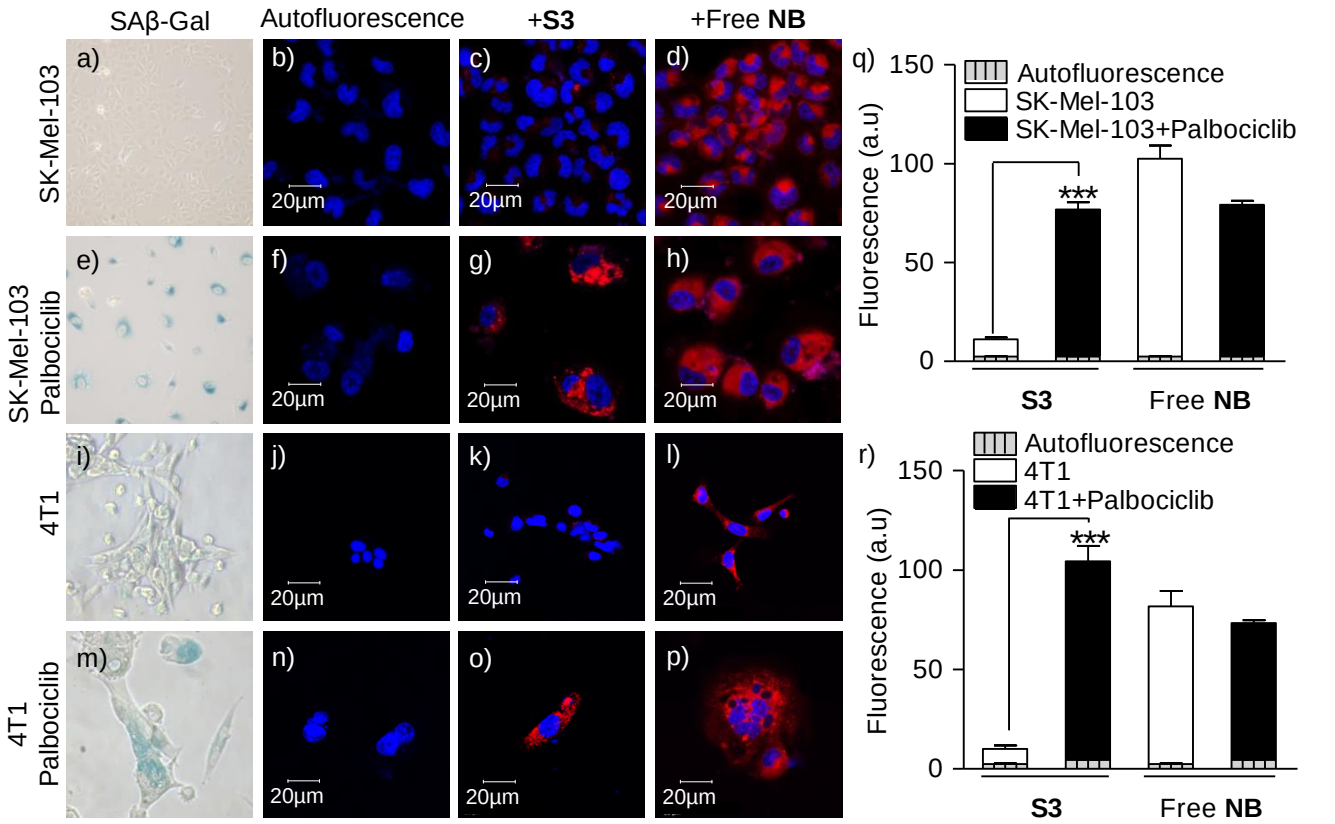

Figure 3. (a,e,i,m) X-Gal assay for detection of SA-β-Gal expression in (a) control and (e) senescent SK-Mel-103 cells and in (i) control 4T1 and (m) senescent 4T1 cells. (b,c) Confocal images of control SK-Mel-103 cells (b) in the absence or (c) in the presence of **S3**. (f,g) SK-Mel-103 cells treated with palbociclib (f) in the absence (g) or in the presence of **S3**. (d,h) Confocal images of (d) control SK-Mel-103 cells or (h) SK-Mel-103 cells treated with palbociclib in the presence of equivalent doses of free **NB**. (j,k) Confocal images of control 4T1 cells (j) in the absence or (k) in the presence of **S3**. (n,o) 4T1 cells treated with palbociclib (n) in the absence (o) or in the presence of **S3**. (l,p) Confocal images of (l) control 4T1 cells or (p) 4T1 treated with palbociclib in the presence of equivalent doses of free **NB**. Cells were incubated with **S3** (7.8 µg/ml) for 4.5 h in DMEM (10% FBS) in 20% O_2 and 5% CO_2 at 37°C, washed three times and stained with Hoechst (1.5 ng/ml) for 15 min. Confocal images were acquired by using confocal microscope (Leica TCS SP8 AOBS). Representative images from repeated experiments (n=3) are shown. (q) Quantification of fluorescence emission ascribed to released **NB** in control and palbociclib-treated SK-Mel-103 cells incubated with **S3** and quantification of fluorescence emission upon treatment with equivalent doses of free **NB**. Autofluorescence is the emission observed in SK-Mel-103 cells without treatment with **S3** or free **NB**. (r) Quantification of fluorescence emission ascribed to released **NB** in control and palbociclib-treated 4T1 cells incubated with **S3** and quantification of fluorescence emission upon treatment with equivalent doses of free **NB**. Autofluorescence is the emission observed in 4T1 cells without treatment with **S3** or free **NB**. Error bars represent s.d.

Confocal microscopy studies of palbociclib-treated SK-Mel-103 and 4T1 cells, incubated with **S3**, revealed an intense fluorescent signal (Figure 3g and 3o), whereas non-senescent SK-Mel-103 and 4T1 cells treated with **S3** presented weak fluorescence (Figure 3c and 3k). Both control and senescent SK-Mel-103 and 4T1 cells showed also negligible background (Figures 3b, 3f, 3j and 3n respectively). In addition, it was found that control and senescent cells treated with equivalent doses of free **NB** presented nearly the same fluorescence (Figures 3d, 3h, 3l and 3p, see also Figure S8). Quantification of fluorescence showed 7-fold emission enhancement in senescent SK-Mel-103 cells treated with **S3** compared to controls (Figure 3q). For the 4T1 cell line, the emission enhancement of senescent cells tretaed with **S3** when compared to control 4T1 cells was 10-fold. Results are indicative of **S3** uptake and galacto-oligosacchadride hydrolysis by SA-β-Gal in senescent cells, resulting in **NB** release. Moreover it was found that **S3** nanoparticles were not toxic for both control and senescent cells (Figure S9).

In vivo detection of celular senescence with **S3** was validated in mice bearing breast tumors treated with senescence-inducing chemotherapy. For this purpose, BALB/cByJ female mice were orthotopically injected with 4T1 (mouse mammary carcinoma) cells (0.5 x 10^6 cell/mouse) to generate breast tumors.

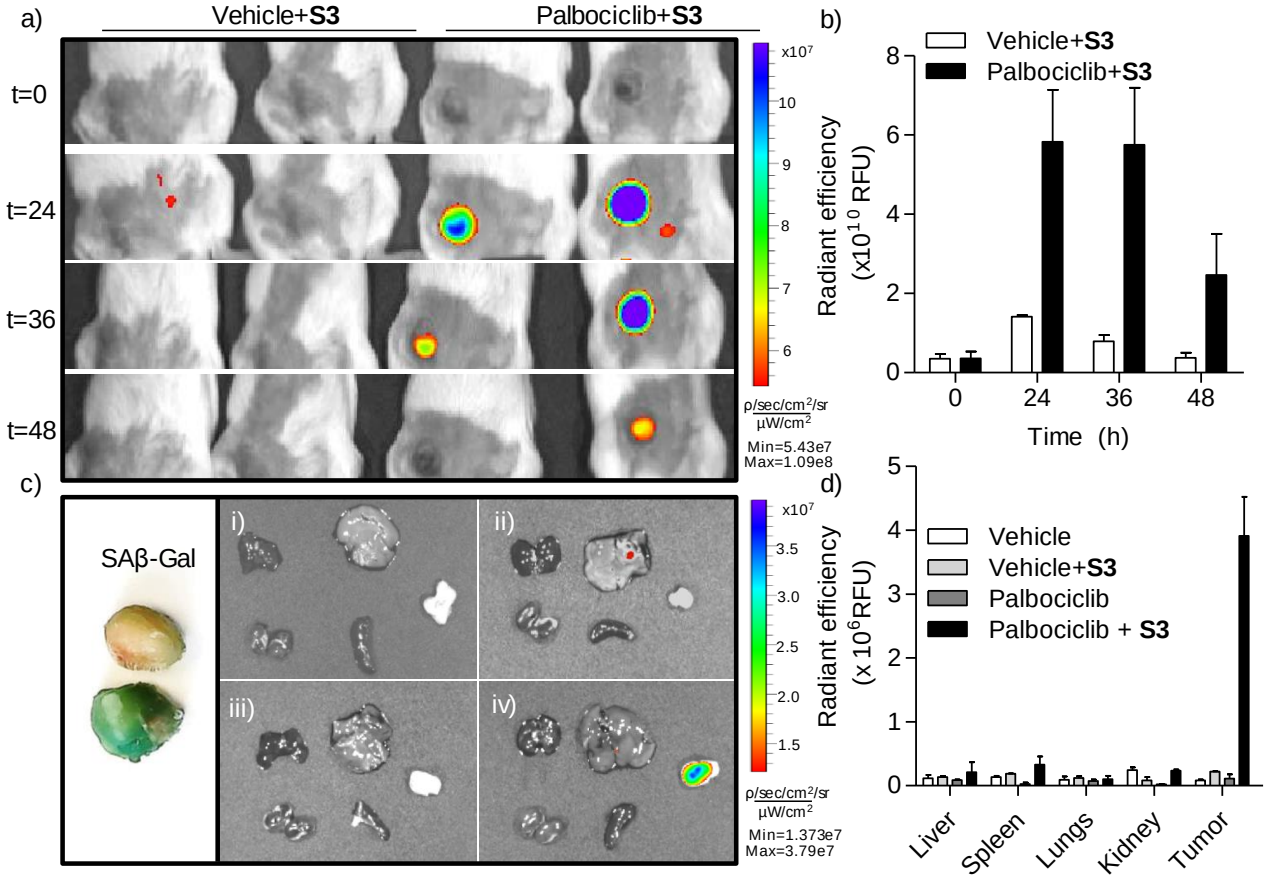

Figure 4. (a) IVIS images at different time points of BALB/cByJ female mice bearing 4T1 breast tumor. From left to right control mice treated with **S3** (two mice from group B) and BALB/cByJ mice treated by oral gavage with palbociclib (senescent tumors) for 1 week and intravenously injected with **S3** (two mice from group D). (b) Quantification of fluorescence emission intensity from tumor signals with time. Error bars represent s.d. (c) X-Gal assay for SA-β-Gal expression in tumors from control group A (up) and palbociclib-treated group C (bottom). (i,ii, iii,iv) IVIS images of organs and tumors from BALB/cByJ female mice bearing 4T1 breast tumor. From left to right and from top to bottom: lungs, liver, tumor, kidney and spleen. (i) Control mice (group A). (ii) Control mice treated with **S3** (group B, 4 mg/ml 200 µl). (iii) BALB/cByJ female mice bearing 4T1 breast tumor treated oral gavage with palbociclib for 1 week (group C). (iv) Palbociclib-treated mice intravenously injected with **S3** (group D, 4 mg/ml 200 µl). Mice were sacrificed 24 h post-treatment for these images. (d) Quantification of fluorescence emission from organs and tumors in i,ii,iii and iv images. Error bars represent s.d.

Mice were divided into four groups: (A) control individuals with 4T1 tumors; (B) control individuals with 4T1 tumors administered with **S3**; (C) mice only administered with palbociclib; and (D) individuals with 4T1 tumors treated with palbociclib and **S3**. Groups C and D were daily treated by oral gavage with palbociclib after tumor development to induce sensecence and arrest of tumor growth. Once completed 7 days of palbociclib treatment, **S3** nanoparticles were intravenously administered to groups B and D, and mice were monitored by an *in vivo* imaging system (IVIS) at different time points for 48 h. No autofluorescence was observed from control (A) and palbociclib (C) treated mice (Figure S10). Mice from groups A, B and C showed negligible fluorescence in the tumor area, while a strong fluorescent signal was observed for group D, which was administered both with palbociclib and **S3** (Figure 4a). The peak of maximum fluorescence in mice treated with palbociclib and **S3** (group D) was observed 24-36 h post-injection of the nanoparticles (Figure 4a), whereas a clear decrease in the fluorescence signal was found at 48 h. Quantification of the relative values of radiance (p/s/cm^2/sr x 10^{10}) showed and enhancement of 4.3 fold at 24 h and 7.3 fold at 36 h in palbociclib+**S3** treated mice when compared to vehicle ones (Figure 4b).

Mice were euthanized and blood, lungs, liver, kidney, spleen and tumors were *ex vivo* analyzed. Senescence in tumors from mice treated with palbociclib was confirmed by X-Gal staining (Figure 4c) and reduced immunostaining of the Ki67 proliferation marker indicative of cell cycle arrest (Figure S11). IVIS images o excised organs and tumors from vehicle (A) or palbociclib-treated mice (C) did not show any fluorescence (Figures 4c, i) and iii)). Similarly, tumors from vehicle mice injected with **S3** (B) did not show any noticeable fluorescent signal (Figure 4c, ii)). In contrast, strong emission (ca. 17.6 fold) was observed in tumors from mice treated with palbociclib and intravenously injected with **S3** (Figure 4c, iv and Figure 4d). Biodistribution of nanoparticles was studied by determining silicon levels in various organs by inductively coupled plasma mass spectroscopy (ICP-MS) (Figure S12). Nanoparticles reach both senescent and non-senescent tumors at 24 h whereas levels of Si are significantly reduced 48 h post-injection, which is consistent with the patterns of fluorescence signal (*vide ante*). **S3** also acumulated in spleen, lungs and kidney at 24 h, whereas maxiumum silicon acumulation was found in spleen at

48 h. Note that even though some mesoporous silica nanoparticles accumulate in liver, spleen or kidney, negligible fluorescence was detected in these organs 24 h post injection. This is due to the very low emission from the capped **S3** (due to π-stacking **NB** interactions in the pores) and also indicates that nanoparticles remain capped in these organs which did not overexpress SA-β-Gal enzyme. Blood biochemistry and hematology analysis of different paremeters, such as albumin (ALB), bilirubin (BIL), alkaline phosphatase (AKP), glutamic pyruvic transaminase (GPT) and aspartate transaminase (GOT), showed no noticeable signs of organ damage and systemic inflammatory response after nanoparticles administration (B and D) when compared to **S3** untreated (A and C) groups (Figure S13).

As summary, we describe here MSN loaded with **NB** dye and capped with a galacto-oligosaccharide for the *in vivo* detection of cellular senescence. **S3** nanoparticles are poorly emissive due to π-stacking interactions of **NB** molecules densely packed onto the mesopores, yet **NB** is selectively released in senescent cells resulting in a marked emission enhancement. *In vitro* targeting of senescent cells with **S3** was validated in SK-Mel-103 and 4T1 cells treated with palbociclib. A remarkable enhanced emission in palbociclib-treated SK-Mel-103 and 4T1 senescent cells was observed when incubated with **S3** in comparison with control cells. **S3** was validated *in vivo* in BALB/cByJ female mice orthotopically injected with 4T1 cells to generate breast tumors and treated with palbociclib. *In vivo* IVIS images showed a remarkable emission enhancement (4.3 fold at 24 h and 7.3 fold at 36 h) in tumors from mice treated with palbociclib and intravenously injected with **S3**, whereas negligible signal was found in mice only treated with **S3** and in palbociclib-treated mice without **S3** administration. In good accordance, *ex vivo* IVIS images showed that fluorescence ascribed to **NB** was only observed in senescent tumors (17.6-fold enhancement) but not in control tumors or other organs. The performance in terms of selectivity and sensitivity makes **S3** and efficient OFF-ON probe for the *in vivo* detection of senescence. We anticipate that this or similar probes able to detect cellular senescence *in vivo* will become essential tools to follow treatment response and efficacy of senotherapies in a wide range of aged-related diseases.

Acknowledgements

R.M thank financial support from the Spanish Government (RTI2018-100910-B-C41 and RTI2018-101599-B-C22 (MCUI/AEI/FEDER, UE)) and the Generalitat Valenciana (PROMETEO 2018/024). M.O. thanks the financial support from SAF2017-84689-R project and MINECO/AEI/FEDER, UE and the Generalitat Valenciana (PROMETEO/2019/065). B.L-T. is grateful to the Spanish Ministry of Economy for her PhD grant. I.G. thanks her contract from IDM. J. F.-B and M. A. thank the UPV for their postdoctoral fellowship.

Keywords: senescence • mesoporous nanoparticles • Nile Blue • NIR • *in vivo* detection

[1] S. He, N. E. Sharpless, *Cell* **2017**, *169*, 1000–1011.

[2] (a) B. Lozano-Torres, A. Estepa-Fernández, M. Rovira, M. Orzáez, M. Serrano, R. Martínez-Máñez, F. Sancenón, *Nat. Rev. Chem.* **2019**, *3*, 426-441; (b) D. Muñoz-Espín, M. Serrano, *Nat. Rev. Mol. Cell Biol.* **2014**, *15*, 482–496.

[3] A. Hernandez-Segura, J. Nehme, M. Demaria, *Trends Cell Biol.* **2018**, *28*, 436–453.

[4] D. J. Baker, B. G. Childs, M. Durik, M. E. Wijers, C. J. Sieben, J.A. Zhong, R. Saltness, K. B. Jeganathan, G. C. Verzosa, A. Pezeshki, K. Khazaie, J. D. Miller, J. M. van Deursen, *Nature* **2016**, *530*, 184–189.

[5] A. Soto-Gamez, M. Demaria, M. *Drug Discov. Today* **2017**, *22*, 786–795.

[6] J. L. Kirkland, T. Tchkonia, Y. Zhu, L. J. Niedernhofer, P. D. Robbins, *J. Am. Geriatr. Soc*. **2017**, *65*, 2297–2301.

[7] L. J. Niedernhofer, P. D. Robbins, *Nat. Rev. Drug Discov.* **2018**, *17*, 377–377.

[8] L. Hayflick, P. S. Moorhead, *Exp. Cell Res.* **1961**, *25*, 585–621.

[9] R. Zhang, P. D. Adams, *Cell Cycle* **2007**, *6*, 784–789.

[10] J. Campisi, *Cell* **2005**, *120*, 513–522.

[11] G. P. Dimri, X. Lee, G. Basile, M. Acosta, G. Scott, C. Roskelley, E. E. Medrano, M. Linskens, I. Rubelj, O. Pereira-Smith, *Proc. Natl. Acad. Sci. U.S.A.* **1995**, *92*, 9363–9367.

[12] B. Lozano-Torres, I. Galiana, M. Rovira, E. Garrido, S. Chaib, A. Bernardos, D. Muñoz-Espín, M. Serrano, R. Martínez-Máñez, F. Sancenón, *J. Am. Chem. Soc.* **2017**, *139*, 8808–8811.

[13] D. Asanuma, M. Sakabe, M. Kamiya, K. Yamamoto, J. Hiratake, M. Ogawa, N. Kosaka, P. L: Choyke, T. Nagano, H. Kobayashi, Y. Urano, *Nat. Commun*. **2015**, *6*, 6463.

[14] D. Muñoz-Espín, *Transl. Med. Aging* **2019**, *3*, 1–5.

[15] A. E. Ekpenyong-Akiba, F. Canfarotta, H. B. Abd, M. Poblocka, M. Casulleras, L. Castilla-Vallmanya, G. Kocsis-Fodor, M. E. Kelly, J. Janus, M. Althubiti, E. Piletska, S. Piletskyc, S. Macip, *Nanoscale Horiz.* **2019**, *4*, 757–768.

[16] (a) S. Alberti, G. Soler-Illia, O. Azzaroni, *Chem. Commun.* **2015**, *51*, 6050-6075; (b) C. de la Torre, I. Casanova, G. Acosta, C. Coll, M.J. Moreno, F. Albericio, E. Aznar, R. Mangues, M. Royo, F. Sancenón, R. Martínez-Máñez, *Adv. Funct. Mater*.**2015**, *25*, 687–695.

[17] (a) A. Bernardos, E. Aznar, M.D. Marcos, R. Martínez-Máñez, F. Sancenón, J. Soto, J.M. Barat, P. Amorós, *Angew. Chem. Int. Ed.* **2009**, *48*, 5884–5887; (b) A. Agostini, L. Mondragón, A. Bernardos, R. Martínez-Máñez, M.D: Marcos, F. Sancenón, J. Soto, A. Costero, C. Manguan-García, R. Perona, M. Moreno-Torres, R. Aparicio-Sanchís, J.R. Murguía, *Angew. Chem. Int. Ed.* **2012**, *51*, 10556–10560; (c) D. Muñoz-Espín, M. Rovira, I. Galiana, C. Giménez, B. Lozano-Torres, M. Paez-Ribes, S. Llanos, S. Chaib, M. Muñoz-Martín, A. C. Ucero, G. Garaulet, F. Mulero, S. G. Dann, T. Van Arsdale, D. J. Shields, A. Bernardos, J. R. Murguía, R. Martínez-Máñez, M. Serrano, *EMBO Mol. Med.* **2018**, e9355.

[18] J. Mérian, J. Gravier, F. Navarro, I. Texier, *Molecules* **2012**, *17*, 5564–5591.

[19] X. Zhang, S. Bloch, W. Akers, S. Achilefu, *Curr Prot. Cytom.* **2012**, *60*, 12.27.1–12.27.20.

[20] W. Fu, C. Yan, Z. Guo, J. Zhang, H. Zhang, H. Tian, W. –H. Zhu, *J. Am. Chem. Soc.* **2019**, *141*, 3171-3177.

[21] O. V. Ovchinnikov, A. V. Evtukhova, T. S. Kondratenko, M. S. Smirnov, V. Y. Khokhlov, O. V. Erina, *Vib. Spectrosc.* **2016**, *86*, 181–189.

[22] (a) E. Aznar, M. Oroval, J. R. Murgía, R. Martínez-Máñez, F. Sancenón, *Chem. Rev.* **2016**, *116*, 561–718; (b) A. Llopis-Lorente, B. Lozano-Torres, A. Bernardos, R. Martínez-Máñez, F. Sancenón, *J. Mater. Chem. B* **2017**, *5*, 3069-3083; (c) A. García-Fernández, E. Aznar, R. Martínez-Máñez, F. Sancenón, *Small* **2020**, *16*, 1902242.

[23] (a) V. Kozlovskaya, B. Xue, E. Kharlampieva, *Macromolecules* **2016**, *49*, 8373-8386; (b) D. K. Mishra, R. Shandilya, P. K. Mishra, *Nanomedicine* **2018**, *14*, 2023-2050; (c) F. Seidi, R. Jenjof, T. Phakkeeree, D. Crespy, *J. Control. Release* **2018**, *284*, 188-212; (d) W. Chen, S. Zhou, L. Ge, W. Wu, X. Jiang, *Biomacromolecules* **2018**, *19*, 1732-1745; (e) M. Vazquez-Gonzalez, I. Willner, *Langmuir* **2018**, *34*, 14692-14710; (f) R. M. Farid, N. A. H. A. Youssef, A. A. Kassem, *Curr. Pharm. Des.* **2017**, *23*, 6613-6629; (g) D. Lombardo, P. Calandra, D. Barreca, S. Magazu, M. A. Kiselev, *Nanomaterials* **2016**, *6*, 125/1-125/26; (h) A. Bansal, Y. Zhang, *Acc. Chem. Res.* **2014**, *47*, 3052-3060; (i) N. Kamaly, B. Yameen, J. Wu, O. C. Farokhzad, *Chem. Rev.* **2016**, *116*, 2602-2663.

[24] B. G. Trewyn, I. I. Slowing, S. Giri, H. –T. Chen, V. S. –Y. Lin, *Acc. Chem. Res.* **2007**, *40*, 846-853.

In vivo detection of cellular senescence using mesoporous silica nanoparticles loaded with Nile Blue and capped with a galacto-hexasaccharide. Fluorescence dye emission is quenched inside nanoparticles, yet a remarkable fluorescence is observed upon cap hydrolysis by β-galactosidase. The probe is able to detect cellular senescence *in vitro* in SK-Mel-103 and 4T1 cells and in *in vivo* palbociclib-treated BALB/cByJ mice bearing breast tumors.

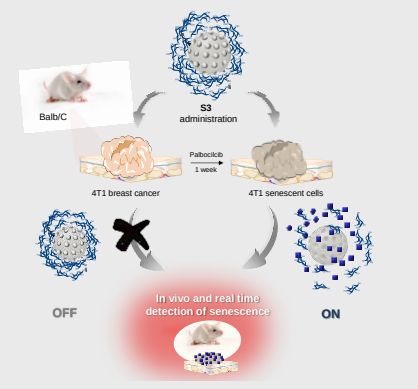

Beatriz Lozano-Torres, Juan F. Blandez, Irene Galiana, María Alfonso, María D. Marcos, Mar Orzaez, Félix Sancenón,* Ramón Martínez-Máñez*.

Page No. – Page No.

Real time *in vivo* detection of cellular senescence through the controlled release of the NIR fluorescent dye Nile Blue